

CONSERVATIVE DISCONTINUOUS GALERKIN/HERMITE SPECTRAL METHOD FOR THE VLASOV-POISSON SYSTEM

FRANCIS FILBET AND TAO XIONG

FRANCIS FILBET

Institut de Mathématiques de Toulouse , Université Paul Sabatier
Toulouse, France

TAO XIONG

School of Mathematical Sciences, Xiamen University
Fujian Provincial Key Laboratory of Math. Mod. & HPSC
Xiamen, Fujian, 361005, P.R. China

ABSTRACT. We propose a class of conservative discontinuous Galerkin methods for the Vlasov-Poisson system written as a hyperbolic system using Hermite polynomials in the velocity variable. These schemes are designed to be systematically as accurate as one wants with provable conservation of mass and possibly total energy. Such properties in general are hard to achieve within other numerical method frameworks for simulating the Vlasov-Poisson system. The proposed scheme employs discontinuous Galerkin discretization for both the Vlasov and the Poisson equations, resulting in a consistent description of the distribution function and electric field. Numerical simulations are performed to verify the order of accuracy and conservation properties.

CONTENTS

1. Introduction	2
2. Hermite spectral form of the Vlasov equation	3
2.1. Hermite basis	4
2.2. Conservation properties	5
2.3. Filtering technique	6
3. Discontinuous Galerkin scheme	6
3.1. Semi-discrete discontinuous Galerkin scheme	7
3.2. Conservation properties for the semi-discrete scheme	8
3.3. Time discretization	11
4. Numerical examples	14
4.1. Landau damping	14
4.2. Two stream instability	16
4.3. Bump-on-tail instability	16
5. Conclusion and perspectives	18
Acknowledgement	18
Conflict of interest	18
References	19

2010 *Mathematics Subject Classification*. Primary: 76P05, 82C40, Secondary: 65N08, 65N35 .

Key words and phrases. energy conserving; discontinuous Galerkin method; Hermite spectral method; Vlasov-Poisson.

1. INTRODUCTION

One of the simplest model that is currently applied in plasma physics simulations is the Vlasov-Poisson system. Such a system describes the evolution of charged particles (electrons and ions) under the effects of a self-consistent electric field. For each species labelled α , the unknown $f_\alpha(t, \mathbf{x}, \mathbf{v})$, depending on the time t , the position \mathbf{x} , and the velocity \mathbf{v} , represents the distribution function of particles in phase space. This model can be used for the study of beam propagation or a collisionless plasma

$$(1.1) \quad \begin{cases} \frac{\partial f_\alpha}{\partial t} + \mathbf{v} \cdot \nabla_{\mathbf{x}} f_\alpha + \frac{q_\alpha}{m_\alpha} \mathbf{E} \cdot \nabla_{\mathbf{v}} f_\alpha = 0, \\ f_\alpha(t=0) = f_{\alpha,0}, \end{cases}$$

where q_α represents the single charge and m_α represents the mass of one particle α , whereas the electric field $\mathbf{E} = -\nabla_{\mathbf{x}}\Phi$ satisfies the Poisson equation

$$(1.2) \quad -4\pi\epsilon_0\Delta_{\mathbf{x}}\Phi = \sum_{\alpha} q_{\alpha}n_{\alpha}, \quad \text{with } n_{\alpha} = \int_{\mathbb{R}^3} f_{\alpha} \, d\mathbf{v},$$

where ϵ_0 is the vacuum permittivity. On the one hand, for a smooth and nonnegative initial data $f_{\alpha,0}$, the solution $f_\alpha(t)$ to (1.1) remains smooth and nonnegative for all $t \geq 0$. On the other hand, for any function $\beta \in C^1(\mathbb{R}^+, \mathbb{R}^+)$, we have

$$\frac{d}{dt} \int_{\mathbb{R}^d \times \mathbb{R}^d} \beta(f_\alpha(t)) \, d\mathbf{x} \, d\mathbf{v} = 0, \quad \forall t \in \mathbb{R}^+,$$

which leads to the conservation of mass, L^p norms, for $1 \leq p \leq +\infty$ and kinetic entropy,

$$\mathcal{H}(t) := \int_{\mathbb{R}^6} f_\alpha(t) \ln(f(t)) \, d\mathbf{x} \, d\mathbf{v} = \mathcal{H}(0), \quad \forall t \geq 0.$$

We also get the conservation of momentum

$$\sum_{\alpha} \int_{\mathbb{R}^6} m_{\alpha} \mathbf{v} f_{\alpha}(t) \, d\mathbf{x} \, d\mathbf{v} = \sum_{\alpha} \int_{\mathbb{R}^6} m_{\alpha} \mathbf{v} f_{\alpha,0} \, d\mathbf{x} \, d\mathbf{v}$$

and total energy

$$\mathcal{E}(t) := \sum_{\alpha} \frac{m_{\alpha}}{2} \int_{\mathbb{R}^6} f_{\alpha}(t) \|\mathbf{v}\|^2 \, d\mathbf{x} \, d\mathbf{v} + 2\pi\epsilon_0 \int_{\mathbb{R}^3} \|\mathbf{E}\|^2 \, d\mathbf{x} = \mathcal{E}(0), \quad \forall t \geq 0.$$

The numerical resolution of the Vlasov-Poisson system (1.1)-(1.2) is often performed by particle methods (PIC) which consist in approximating the plasma by a finite number of macro-particles. The trajectories of these particles are computed from the characteristic curves given by the Vlasov equation, whereas self-consistent fields are computed on a mesh of the physical space. This method allows to obtain satisfying results with a few number of particles (we refer to Birdsall-Langdon for more details [4]). However, it suffers from poor accuracy since the numerical noise only decreases in $1/\sqrt{N}$ when the number of particles N is increased, which is not satisfying for some specific problems. Therefore, different approaches, discretizing the Vlasov equation on a mesh of phase space, have been proposed. Among them, the Fourier-Fourier transform is based on a Fast Fourier Transform of the distribution function in phase space, but this method is only valid for periodic boundary conditions [25]. Consequently, for non periodic boundary conditions, Gibbs oscillations form at the boundary of the grid and become source of spurious oscillations which propagate into the distribution function. Later semi-Lagrangian methods, which consist in computing the distribution function at each grid point by following the characteristic curves backward, were also used. To compute the origin of the characteristics, a high order interpolation method is needed. E. Sonnendrücker *et al.* proposed the cubic spline reconstruction which gives very good results [31], but the use of spline interpolation destroys the local character of the reconstruction. Nakamura and Yabe also presented the Cubic Interpolated Propagation (CIP) method based on the approximation of the gradients of the distribution function in order to use a Hermite interpolation [32]. This method is very expensive

in memory computation since it needs the storage of f , $\nabla_x f$, and $\nabla_v f$. Another scheme for the Vlasov equation is the Flux Corrected Transport (FCT) [5] or more recently finite volume methods [17, 16, 13, 30]: the basic idea is to compute the average of the Vlasov equation solution in each cell of the phase space grid by a conservative method. In the sixties, a variant has been proposed: rather to discretize the function in velocity space, Galerkin methods with a small finite set of orthogonal polynomials are used [1, 24]. More recently, in [33, 22] and [29], the authors have shown the merit to use rescaled orthogonal basis like the so-called scaled Hermite basis. In [29], the authors show that, according to some symmetry properties of the Hermite weights, the numerical method conserves certain integral quantities like the number of particles, the momentum, the energy or the L^2 -norm. These properties lead to algorithms that can provide long time numerical stability while using a small set of basis functions. The aim of the present work is to apply these techniques in order to handle with the velocity space and design conservative discretization with a reduced degree of freedom.

For the space discretization, we adopt the point of view of discontinuous Galerkin methods. These methods are similar to finite element methods but use discontinuous polynomials and are particularly well suited to handle complicated boundaries which may arise in many practical applications. Moreover, their local construction endows the methods with good local conservation properties without sacrificing the order of accuracy. Furthermore, they are extremely flexible in handling hp -adaptivity, the boundary conditions are imposed weakly and the mass matrices are block-diagonal which results in very efficient time-stepping algorithms in the context of time-dependent problems, as it is the case here. Among the computational works, we mention the use of discontinuous Galerkin schemes for the Vlasov-Poisson system in [11, 20]; and Vlasov-Maxwell [10]. Several theoretical works have been performed to analyze a family of semi-discrete discontinuous Galerkin schemes for the Vlasov-Poisson system with periodic boundary conditions, for the one [2] and multi-dimensional cases [3], but also for the Vlasov-Maxwell system [35]. The authors show optimal error estimates for both the distribution function and the electrostatic field, and they study the conservation properties of the proposed schemes. Let us emphasize that these former works apply a discontinuous Galerkin method using a phase space mesh, whereas here we adopt this approach only in physical space. Furthermore, we propose to modify the fluxes to ensure conservation of mass, momentum and total energy. We prove these conservations for the semi-discrete and fully discrete cases (first and second order time discretizations).

This paper is organized as follows: in the first part (Section 2), we briefly reformulate the Vlasov equation using the Hermite basis in velocity, recalling some properties of the solution. Then, in Section 3, we present a variant of the discontinuous Galerkin method for the space discretization such that mass, momentum and energy are preserved for semi-discrete and fully discrete systems. In the last section (Section 4), we present numerical results for Landau damping, two stream instability and bump on the tail problems to illustrate accuracy and conservations of our discretization technique.

2. HERMITE SPECTRAL FORM OF THE VLASOV EQUATION

For simplicity, we now set all the physical constants to one and consider the one dimensional Vlasov-Poisson system for a single species with periodic boundary conditions in space, where the Vlasov equation reads

$$(2.1) \quad \frac{\partial f}{\partial t} + v \frac{\partial f}{\partial x} + E \frac{\partial f}{\partial v} = 0$$

with $t \geq 0$, position $x \in (0, L)$ and velocity $v \in \mathbb{R}$. Moreover, the self-consistent electric field E is determined by the Poisson equation

$$(2.2) \quad \frac{\partial E}{\partial x} = \rho - \rho_0,$$

where the density ρ is given by

$$\rho(t, x) = \int_{\mathbb{R}} f(t, x, v) \, dv, \quad t \geq 0, \, x \in (0, L)$$

and ρ_0 is a constant ensuring the quasi-neutrality condition of the plasma

$$(2.3) \quad \int_0^L (\rho - \rho_0) dx = 0.$$

2.1. Hermite basis. To discretize the velocity variable, our approach is based on spectral methods, where we expand the velocity part of the distribution function in basis functions (typically Fourier or Hermite), leading to a truncated set of moment equations for the expansion coefficients. Actually, spectral methods are commonly used to approximate the solution to partial differential equations [6, 21] and in particular the Vlasov-Poisson system [28, 25, 14, 22, 29].

For instance, in their seminal work [28], M. Shoucri and G. Knorr applied Chebyshev polynomials, whereas in [25, 14] the authors used Fourier basis but these methods does not conserve neither momentum, nor total energy. Later, J. P. Holloway and J. W. Schumer [22, 29] applied Hermite functions. Indeed, the product of Hermite polynomials and a Gaussian, seems to be a natural choice for Maxwellian-type velocity profiles [19]. Moreover, compared with other classical polynomials, they possess a fairly simple expression for their derivatives and allow to get conservation of mass, momentum and total energy. Recently, these methods generate a new interest leading to new techniques to improve their efficiency [26, 7, 9, 27, 8, 12].

Let us summarize the main characteristics of this approach. The solution f is approximated by a finite sum which corresponds to a truncation of a series

$$(2.4) \quad f(t, x, v) = \sum_{n=0}^{N_H-1} C_n(t, x) \Psi_n(v),$$

where N_H is the number of modes. The issue is then to determine a well-suited class of basis functions Ψ_n and to find the expansion coefficients C_n . Here, we have chosen the following basis of normalized scaled asymmetrically weighted Hermite functions:

$$(2.5) \quad \Psi_n(v) = H_n \left(\frac{v}{v_{th}} \right) \frac{e^{-v^2/2v_{th}^2}}{\sqrt{2\pi}},$$

where v_{th} corresponds to the scaling velocity and we have set $H_{-1}(\xi) = 0$, $H_0(\xi) = 1$ and for $n \geq 1$, $H_n(\xi)$ has the following recursive relation

$$(2.6) \quad \sqrt{n} H_n(\xi) = \xi H_{n-1}(\xi) - \sqrt{n-1} H_{n-2}(\xi), \quad \forall n \geq 1.$$

The Hermite basis (2.5) has the following properties

$$(2.7) \quad \int_{\mathbb{R}} \Psi_n(\xi) \Psi_m(\xi) \frac{e^{\xi^2/2}}{\sqrt{2\pi}} d\xi = \delta_{n,m},$$

and $\delta_{n,m}$ is the Kronecker delta function. With those properties, one can substitute the expression (2.4) for f into the Vlasov equation (2.1) and using the orthogonality property (2.7), it yields an evolution equation for each mode C_n ,

$$(2.8) \quad \frac{\partial C_n}{\partial t} + v_{th} \left(\sqrt{n+1} \frac{\partial C_{n+1}}{\partial x} + \sqrt{n} \frac{\partial C_{n-1}}{\partial x} \right) - \frac{\sqrt{n}}{v_{th}} E C_{n-1} = 0.$$

Meanwhile, we first observe that the density ρ satisfies

$$\rho = \int_{\mathbb{R}} f dv = v_{th} C_0,$$

then the Poisson equation becomes

$$(2.9) \quad \frac{\partial E}{\partial x} = v_{th} C_0 - \rho_0.$$

Observe that if we take $N_H = \infty$ in the expression (2.4), we get an infinite system (2.8)-(2.9) of equations for $(C_n)_{n \in \mathbb{N}}$ and E , which is formally equivalent to the Vlasov-Poisson system (2.1)-(2.2).

2.2. Conservation properties. There are different kinds of Hermite approximations based on the choice of Hermite functions and weights. In [22, 29], J. W. Schumer and J. P. Holloway have discussed precisely the different choices of orthogonal Hermite basis functions depending on the form of their weight functions. If the basis is asymmetrically weighted, hence mass, momentum and total energy are preserved but not the L^2 norm. In the case of symmetrically weighted basis functions, particles number, total energy (for N_H odd) or momentum (for N_H even), as well as L^2 -norm are conserved and the numerical stability is shown to be better. Moreover, it has been shown in [33] and later in [26] that it is required to introduce a velocity scaling factor to make the method more accurate and stable. Here, the basis is asymmetrically weighted, hence we prove the following result for the truncated system (2.8)-(2.9).

Proposition 2.1. *For any $N_H \in \mathbb{N}$, consider the distribution function f given by the truncated series*

$$f(t, x, v) = \sum_{n=0}^{N_H-1} C_n(t, x) \Psi_n(v),$$

where (C_n, E) is a solution to the Vlasov-Poisson system written as (2.8)-(2.9). Then mass, momentum and total energy are conserved, that is,

$$v_{th}^{k+1} \frac{d}{dt} \int_0^L C_k dx = 0, \quad k = 0, 1$$

and for the total energy,

$$\mathcal{E}(t) := \frac{1}{2} \int_0^L v_{th}^3 (\sqrt{2} C_2 + C_0) + |E|^2 dx = \mathcal{E}(0).$$

Proof. We consider the first three equations of (2.8) given by

$$(2.10) \quad \begin{cases} \frac{\partial C_0}{\partial t} + v_{th} \frac{\partial C_1}{\partial x} = 0, \\ \frac{\partial C_1}{\partial t} + v_{th} \left(\sqrt{2} \frac{\partial C_2}{\partial x} + \frac{\partial C_0}{\partial x} \right) - \frac{1}{v_{th}} E C_0 = 0, \\ \frac{\partial C_2}{\partial t} + v_{th} \left(\sqrt{3} \frac{\partial C_3}{\partial x} + \sqrt{2} \frac{\partial C_1}{\partial x} \right) - \frac{\sqrt{2}}{v_{th}} E C_1 = 0, \end{cases}$$

which will be related to the conservation of mass, momentum and energy. Thus, let us take a look at the conservation properties from (2.10), by considering periodic or compact support boundary conditions.

First the total mass is defined as

$$\int_0^L \int_{-\infty}^{\infty} f(t, x, v) dv dx = v_{th} \int_0^L C_0(t, x) dx,$$

hence the conservation of mass directly comes from (2.10) by integrating the first equation with respect to $x \in (0, L)$.

Then we define the momentum as

$$\int_0^L \int_{-\infty}^{\infty} v f(t, x, v) dv dx = v_{th}^2 \int_0^L C_1(t, x) dx,$$

due to the second equation (2.10) and using the Poisson equation (2.9), we get

$$v_{th}^2 \frac{d}{dt} \int_0^L C_1 dx = v_{th} \int_0^L E C_0 dx = \int_0^L E \left(\frac{\partial E}{\partial x} + \rho_0 \right) dx = \rho_0 \int_0^L E dx = 0,$$

so that the conservation of momentum is obtained.

Finally to prove the conservation of total energy W , we compute the variation of the kinetic energy defined as

$$\frac{1}{2} \int_0^L \int_{-\infty}^{\infty} v^2 f(t, x, v) dx dv = \frac{v_{th}^3}{2} \int_0^L (\sqrt{2} C_2 + C_0) dx.$$

Thus, combining the first and third equations in (2.10) and integrating over $x \in (0, L)$, we get

$$(2.11) \quad \frac{v_{th}^3}{2} \frac{d}{dt} \int_0^L (\sqrt{2} C_2 + C_0) dx = v_{th}^2 \int_0^L E C_1 dx.$$

On the other hand, multiplying the first equation in (2.10) by $v_{th} \Phi$ and integrating over $x \in (0, L)$, it yields

$$v_{th} \int_0^L \frac{\partial C_0}{\partial t} \Phi dx = -v_{th}^2 \int_0^L \frac{\partial C_1}{\partial x} \Phi dx = -v_{th}^2 \int_0^L C_1 E dx.$$

Using the Poisson equation (2.9), we have $v_{th} C_0 = -\partial_{xx} \Phi + \rho_0$, hence

$$\frac{1}{2} \frac{d}{dt} \int_0^L |E|^2 dx = \int_0^L \frac{\partial}{\partial t} \left(-\frac{\partial^2 \Phi}{\partial x^2} \right) \Phi dx = -v_{th}^2 \int_0^L C_1 E dx.$$

Combining this latter equality with (2.11), it yields the conservation of total energy

$$\frac{1}{2} \frac{d}{dt} \int_0^L v_{th}^3 (\sqrt{2} C_2 + C_0) + |E|^2 dx = 0.$$

□

Remark 2.2. *The natural space associated to our asymmetrically weighted basis is*

$$L_\omega^2 = \left\{ u : \mathbb{R} \mapsto \mathbb{R} : \int_{\mathbb{R}} |u(v)|^2 e^{|v|^2/2v_{th}^2} dv < \infty \right\}.$$

Unfortunately there is no estimate of the associated norm for the solution to the Vlasov-Poisson system (2.1)-(2.2), hence there is no warranty to get such estimate for the system (2.8)-(2.9). It is worth to mention that the symmetrically weighted basis with the $L^2(\mathbb{R})$ norm would be a good choice, but it would affect the efficiency of the conservation algorithm which will be proposed in the Section 3 (see Remark 3.2).

2.3. Filtering technique. Filtering is a common procedure to reduce the effects of the Gibbs phenomenon inherent to spectral methods [21]. The filter will consist in multiplying some spectral coefficients in (2.4) by a scaling factor σ in order to reduce the amplitude of high frequencies, for any $N_H \geq 4$,

$$\tilde{C}_n = C_n \sigma \left(\frac{n}{N_H} \right).$$

Here, we simply apply a filter, called Hou-Li's filter, already proposed in [23] for Fourier spectral method, which reads

$$\sigma(s) = \begin{cases} 1, & \text{if } 0 \leq |s| \leq 2/3, \\ \exp(-\beta |s|^\beta), & \text{if } |s| > 2/3, \end{cases}$$

where the coefficient β is chosen as $\beta = 36$. Actually this filter achieved great success in Fourier [23] and Hermite [12] spectral methods. We again refer to [12] for a detailed discussion on the application to the Vlasov-Poisson system using a Hermite spectral method.

Remark 2.3. *Observe that the filter is applied only when $N_H \geq 4$, hence the filtering process does not modify the coefficients $(C_k)_{0 \leq k \leq 2}$, that is, conservations of mass, momentum and total energy are not affected.*

3. DISCONTINUOUS GALERKIN SCHEME

This section is devoted to the space and time discretizations of the Vlasov-Poisson system written in the form (2.8)-(2.9). We apply a local discontinuous Galerkin method for space and introduce a slight modification of the fluxes to preserve mass, momentum and local energy for this semi-discrete system. Then, we focus on the time discretization and prove the conservation for the fully-discrete case.

3.1. Semi-discrete discontinuous Galerkin scheme. In this section, we will define the discontinuous Galerkin (DG) scheme for the Vlasov-Poisson system with Hermite spectral basis in velocity (2.8)-(2.9).

Let us first introduce some notations and start with $\{x_{i+\frac{1}{2}}\}_{i=0}^{i=N_x}$, a partition of $\Omega = [x_{\min}, x_{\max}]$. Here $x_{\frac{1}{2}} = x_{\min}$, $x_{N_x+\frac{1}{2}} = x_{\max}$. Each element is denoted as $I_i = [x_{i-\frac{1}{2}}, x_{i+\frac{1}{2}}]$ with its length h_i , and $h = \max_i h_i$.

Given any non-negative integer k , we define a finite dimensional discrete piece-wise polynomial space

$$V_h^k = \{u \in L^2(\Omega) : u|_{I_i} \in P_k(I_i), \forall i\},$$

where the local space $P_k(I)$ consists of polynomials of degree at most k on the interval I . We further denote the jump $[u]_{i+\frac{1}{2}}$ and the average $\{u\}_{i+\frac{1}{2}}$ of u at $x_{i+\frac{1}{2}}$ defined as,

$$[u]_{i+\frac{1}{2}} = u(x_{i+\frac{1}{2}}^+) - u(x_{i+\frac{1}{2}}^-) \quad \text{and} \quad \{u\}_{i+\frac{1}{2}} = \frac{1}{2} \left(u(x_{i+\frac{1}{2}}^+) + u(x_{i+\frac{1}{2}}^-) \right), \quad \forall i,$$

where $u(x^\pm) = \lim_{\Delta x \rightarrow 0^\pm} u(x + \Delta x)$. We also denote

$$\begin{cases} u_{i+\frac{1}{2}} = u(x_{i+\frac{1}{2}}), \\ u_{i+\frac{1}{2}}^\pm = u(x_{i+\frac{1}{2}}^\pm). \end{cases}$$

From these notations, we apply a semi-discrete discontinuous Galerkin method for (2.8) as follows. We look for an approximation $C_{n,h}(t, \cdot) \in V_h^k$, such that for any $\phi_n \in V_h^k$, we have

$$(3.1) \quad \frac{d}{dt} \int_{I_j} C_{n,h} \phi_n \, dx + a_n^j(g_n, \phi_n) - \frac{\sqrt{n}}{v_{th}} \int_{I_j} E C_{n-1,h} \phi_n \, dx = 0, \quad 0 \leq n \leq N_H - 1,$$

where a_n^j is defined as

$$(3.2) \quad \begin{cases} a_n^j(g_n, \phi_n) = - \int_{I_j} g_n \phi_n' \, dx + \hat{g}_{n,j+\frac{1}{2}} \phi_{n,j+\frac{1}{2}}^- - \hat{g}_{n,j-\frac{1}{2}} \phi_{n,j-\frac{1}{2}}^+, \\ g_n = v_{th} (\sqrt{n+1} C_{n+1,h} + \sqrt{n} C_{n-1,h}). \end{cases}$$

The numerical flux \hat{g}_n in (3.2) could be taken as any consistent numerical fluxes. As an example, the global Lax-Friedrichs flux is used, which is defined as

$$(3.3) \quad \hat{g}_n = \frac{1}{2} \left[g_n^- + g_n^+ - \alpha (C_{n,h}^+ - C_{n,h}^-) \right],$$

with the numerical viscosity coefficient $\alpha = v_{th} \sqrt{N_H}$.

For the Poisson equation (2.9), we introduce the potential function $\Phi(t, x)$, such that

$$\begin{cases} E = -\frac{\partial \Phi}{\partial x}, \\ \frac{\partial E}{\partial x} = v_{th} C_0 - \rho_0. \end{cases}$$

Hence we get the one dimensional Poisson equation

$$-\frac{\partial^2 \Phi}{\partial x^2} = v_{th} C_0 - \rho_0,$$

for which we also define a local discontinuous Galerkin scheme: we look for a couple $\Phi_h(t, \cdot), E_h(t, \cdot) \in V_h^k$, such that for any η and $\zeta \in V_h^k$, we have

$$(3.4) \quad \begin{cases} + \int_{I_j} \Phi_h \eta' \, dx - \hat{\Phi}_{h,j+\frac{1}{2}} \eta_{j+\frac{1}{2}}^- + \hat{\Phi}_{h,j-\frac{1}{2}} \eta_{j-\frac{1}{2}}^+ = \int E_h \eta \, dx, \\ - \int_{I_j} E_h \zeta' \, dx + \hat{E}_{h,j+\frac{1}{2}} \zeta_{j+\frac{1}{2}}^- - \hat{E}_{h,j-\frac{1}{2}} \zeta_{j-\frac{1}{2}}^+ = \int (v_{th} C_{0,h} - \rho_0) \zeta \, dx, \end{cases}$$

where the numerical fluxes $\hat{\Phi}_h$ and \hat{E}_h in (3.4) here are taken as in [2, 3],

$$(3.5) \quad \begin{cases} \hat{\Phi}_h = \{\Phi_h\}, \\ \hat{E}_h = \{E_h\} - \beta[\Phi_h], \end{cases}$$

with β either being a positive constant or a constant multiplying by $1/h$ and h is the mesh size.

3.2. Conservation properties for the semi-discrete scheme. The local discontinuous Galerkin method presented in the previous section naturally preserves the mass since the equation on C_0 only contains a convective term. Unfortunately, the momentum and total energy are not conserved due to the contribution of the source terms in (3.1). Therefore, we propose a slight modification of the fluxes for the unknowns (C_1, C_2) in order to ensure the right conservations.

In this subsection, without any confusion, we will drop the subindex h for simplicity. The aim is to modify the scheme (3.1)-(3.5) in order to ensure the conservation of mass, momentum and energy without deteriorating the order of accuracy. Thus, we follow the proof of Proposition 2.1 and consider the scheme (3.1) for $n = 1, 2$ combined with (3.4), by adding two residual terms to ensure the conservation of momentum and total energy

$$(3.6) \quad \begin{cases} \frac{d}{dt} \int_{I_j} C_1 \phi_1 \, dx + a_1^j(g_1, \phi_1) - \frac{1}{v_{th}} \int_{I_j} E C_0 \phi_1 \, dx = \langle r_1^j, \phi_1 \rangle, \\ \frac{d}{dt} \int_{I_j} C_2 \phi_2 \, dx + a_2^j(g_2, \phi_2) - \frac{\sqrt{2}}{v_{th}} \int_{I_j} E C_1 \phi_2 \, dx = \langle r_2^j, \phi_2 \rangle, \end{cases}$$

and the residual terms (r_1, r_2) are given by

$$(3.7) \quad \begin{cases} \langle r_1^j, \phi_1 \rangle = -\frac{\beta}{2v_{th}^2} \left([\Phi][E]_{j-\frac{1}{2}} \phi_{1,j-\frac{1}{2}}^+ + [\Phi][E]_{j+\frac{1}{2}} \phi_{1,j+\frac{1}{2}}^- \right), \\ \langle r_2^j, \phi_2 \rangle = \frac{1}{\sqrt{2}v_{th}} \left((\{C_1\} - \hat{C}_1) [\Phi]_{j-\frac{1}{2}} \phi_{2,j-\frac{1}{2}}^+ + (\{C_1\} - \hat{C}_1) [\Phi]_{j+\frac{1}{2}} \phi_{2,j+\frac{1}{2}}^- \right). \end{cases}$$

Apparently, these residues are given as products of two cell interface jump terms, which both are of high order, hence it should not deteriorate the order of accuracy. Therefore, we prove that this choice will ensure the discrete conservation properties of the scheme.

Proposition 3.1. *For any $N_H \geq 3 \in \mathbb{N}$, we consider the solution (C_n, E, Φ) to the system (3.1)-(3.5) combined with the residual terms (3.6)-(3.7). Then, discrete mass and momentum are conserved*

$$v_{th}^{k+1} \frac{d}{dt} \int_0^L C_k \, dx = 0, \quad k = 0, 1$$

and the discrete total energy, defined as

$$\mathcal{E}_h(t) := \frac{1}{2} \int_0^L v_{th}^3 (\sqrt{2} C_2 + C_0) + |E|^2 \, dx + \frac{1}{2} \beta \sum_j [\Phi]_{j-\frac{1}{2}}^2,$$

is also preserved with respect to time.

Proof. On the one hand, the conservation of mass easily follows by choosing $\phi_0 = 1$ in (3.1) for $n = 0$ and summing over j , hence since there is no source term we get

$$\sum_j \frac{d}{dt} \int_{I_j} C_0 \, dx = 0.$$

On the other hand, for the conservation of momentum, taking $\phi_1 = 1$ in the modified scheme (3.6) and summing over j , we have

$$(3.8) \quad \frac{d}{dt} \int_0^L C_1 \, dx = \frac{1}{v_{th}} \int_0^L E C_0 \, dx + \sum_j \langle r_1^j, 1 \rangle,$$

where the contribution of the residual term, using periodic boundary conditions, gives

$$(3.9) \quad \sum_j \langle r_1^j, 1 \rangle = - \sum_j \frac{\beta}{2 v_{th}^2} \left([\Phi] [E]_{j-\frac{1}{2}} + [\Phi] [E]_{j+\frac{1}{2}} \right) = - \frac{\beta}{v_{th}^2} \sum_j [\Phi] [E]_{j-\frac{1}{2}}.$$

Then we compute the contribution of the first source term on the right hand side of (3.8). Choosing $\eta = 1$ in the first equation of (3.4), we get that

$$\int_{I_j} E \, dx = -\hat{\Phi}_{j+\frac{1}{2}} + \hat{\Phi}_{j-\frac{1}{2}},$$

whereas taking $\zeta = E$ in the second equation of (3.4), we have

$$- \int_{I_j} E \frac{\partial E}{\partial x} \, dx + \hat{E}_{j+\frac{1}{2}} E_{j+\frac{1}{2}}^- - \hat{E}_{j-\frac{1}{2}} E_{j-\frac{1}{2}}^+ = \int_{I_j} (v_{th} C_0 - \rho_0) E \, dx,$$

hence adding the latter both equalities, it yields

$$\begin{aligned} v_{th} \int_{I_j} E C_0 \, dx &= -\frac{1}{2} \int_{I_j} \frac{\partial E^2}{\partial x} \, dx + \hat{E}_{j+\frac{1}{2}} E_{j+\frac{1}{2}}^- - \hat{E}_{j-\frac{1}{2}} E_{j-\frac{1}{2}}^+ + \rho_0 \int_{I_j} E \, dx \\ &= -\frac{1}{2} (E^2)_{j+\frac{1}{2}}^- + \frac{1}{2} (E^2)_{j-\frac{1}{2}}^+ + \hat{E}_{j+\frac{1}{2}} E_{j+\frac{1}{2}}^- - \hat{E}_{j-\frac{1}{2}} E_{j-\frac{1}{2}}^+ + \rho_0 (\hat{\Phi}_{j+\frac{1}{2}} - \hat{\Phi}_{j-\frac{1}{2}}). \end{aligned}$$

Summing on j , we obtain

$$(3.10) \quad v_{th} \int_0^L E C_0 \, dx = \sum_j \left(\frac{1}{2} [E^2] - \hat{E} [E] \right)_{j-\frac{1}{2}} = \sum_j \left(\{E\} - \hat{E} \right)_{j-\frac{1}{2}} [E]_{j-\frac{1}{2}}.$$

Finally, using the definition of the flux \hat{E} in (3.5), we have

$$\left(\{E\} - \hat{E} \right)_{j-\frac{1}{2}} [E]_{j-\frac{1}{2}} = \beta [\Phi] [E]_{j-\frac{1}{2}},$$

hence gathering (3.9) and (3.10) in (3.8), we get the conservation of momentum

$$\frac{d}{dt} \int_0^L C_1 \, dx = 0.$$

Now let us show the conservation of total energy. Choosing $\phi_2 = 1$ in the modified scheme (3.6) and summing over j , we get

$$(3.11) \quad \frac{d}{dt} \int_0^L C_2 \, dx = \frac{\sqrt{2}}{v_{th}} \int_0^L E C_1 \, dx + \sum_j \langle r_2^j, 1 \rangle,$$

where the contribution of the residual term, using periodic boundary conditions, gives

$$(3.12) \quad \sum_j \langle r_2^j, 1 \rangle = \frac{\sqrt{2}}{v_{th}} \sum_j \left((\{C_1\} - \hat{C}_1) [\Phi] \right)_{j-\frac{1}{2}}.$$

Let us evaluate the first term on the right hand side of (3.11). We consider the first equation of (3.4) and take $\eta = C_1$,

$$\int_{I_j} E C_1 \, dx = \int_{I_j} \Phi \frac{\partial C_1}{\partial x} \, dx - \hat{\Phi}_{j+\frac{1}{2}} (C_1)_{j+\frac{1}{2}}^- + \hat{\Phi}_{j-\frac{1}{2}} (C_1)_{j-\frac{1}{2}}^+,$$

whereas in (3.1), we choose $\phi_0 = \Phi/v_{th}$,

$$\frac{1}{v_{th}} \int_{I_j} \frac{\partial C_0}{\partial t} \Phi \, dx = \int_{I_j} C_1 \frac{\partial \Phi}{\partial x} \, dx - \hat{C}_{1,j+\frac{1}{2}} \Phi_{j+\frac{1}{2}}^- + \hat{C}_{1,j-\frac{1}{2}} \Phi_{j-\frac{1}{2}}^+.$$

Adding the latter two equalities, it yields

$$\begin{aligned}
& \int_{I_j} E C_1 + \frac{1}{v_{th}} \frac{\partial C_0}{\partial t} \Phi \, dx \\
&= \int_{I_j} \frac{\partial(\Phi C_1)}{\partial x} \, dx - \hat{\Phi}_{j+\frac{1}{2}} (C_1)_{j+\frac{1}{2}}^- + \hat{\Phi}_{j-\frac{1}{2}} (C_1)_{j-\frac{1}{2}}^+ - \hat{C}_{1,j+\frac{1}{2}} \Phi_{j+\frac{1}{2}}^- + \hat{C}_{1,j-\frac{1}{2}} \Phi_{j-\frac{1}{2}}^+ \\
&= (\Phi C_1)_{j+\frac{1}{2}}^- - (\Phi C_1)_{j-\frac{1}{2}}^+ - \hat{\Phi}_{j+\frac{1}{2}} (C_1)_{j+\frac{1}{2}}^- + \hat{\Phi}_{j-\frac{1}{2}} (C_1)_{j-\frac{1}{2}}^+ - \hat{C}_{1,j+\frac{1}{2}} \Phi_{j+\frac{1}{2}}^- + \hat{C}_{1,j-\frac{1}{2}} \Phi_{j-\frac{1}{2}}^+.
\end{aligned}$$

Summing on j and using periodic boundary conditions, we get

$$\int_0^L \left[E C_1 + \frac{1}{v_{th}} \frac{\partial C_0}{\partial t} \Phi \right] \, dx = - \sum_j \left([\Phi C_1] - \hat{\Phi} [C_1] - \hat{C}_1 [\Phi] \right)_{j-\frac{1}{2}}.$$

To evaluate the right hand side of the latter term, we use that

$$[\Phi C_1] - \hat{\Phi} [C_1] - \hat{C}_1 [\Phi] = \left(\{\Phi\} - \hat{\Phi} \right) [C_1] + \left(\{C_1\} - \hat{C}_1 \right) [\Phi],$$

and from the definition of the flux for the Poisson equation (3.5), we get

$$(3.13) \quad \frac{\sqrt{2}}{v_{th}} \int_0^L \left[E C_1 + \frac{1}{v_{th}} \frac{\partial C_0}{\partial t} \Phi \right] \, dx = - \frac{\sqrt{2}}{v_{th}} \sum_j \left(\left(\{C_1\} - \hat{C}_1 \right) [\Phi] \right)_{j-\frac{1}{2}}.$$

Now, it remains to evaluate the second term on the left hand side in (3.13), hence we compute the time derivative of the second equation in (3.4) and choose the test function $\zeta = \sqrt{2} \Phi / v_{th}^3$, it gives

$$\frac{\sqrt{2}}{v_{th}^2} \int_{I_j} \frac{\partial C_0}{\partial t} \Phi \, dx = \frac{\sqrt{2}}{v_{th}^3} \left[- \int_{I_j} \frac{\partial E}{\partial t} \frac{\partial \Phi}{\partial x} \, dx + \left(\frac{\partial E}{\partial t} \right)_{j+\frac{1}{2}}^- \Phi_{j+\frac{1}{2}}^- - \left(\frac{\partial E}{\partial t} \right)_{j-\frac{1}{2}}^+ \Phi_{j-\frac{1}{2}}^+ \right].$$

Then in the first equation of (3.4), we take $\eta = -\frac{\sqrt{2}}{v_{th}^3} \frac{\partial E}{\partial t}$ and obtain

$$\begin{aligned}
-\frac{1}{\sqrt{2} v_{th}^3} \frac{d}{dt} \int_{I_j} E^2 \, dx &= -\frac{\sqrt{2}}{v_{th}^3} \int_{I_j} E \frac{\partial E}{\partial t} \, dx \\
&= -\frac{\sqrt{2}}{v_{th}^3} \left(\int_{I_j} \Phi \frac{\partial^2 E}{\partial t \partial x} \, dx - \hat{\Phi}_{j+\frac{1}{2}} \left(\frac{\partial E}{\partial t} \right)_{j+\frac{1}{2}}^- + \hat{\Phi}_{j-\frac{1}{2}} \left(\frac{\partial E}{\partial t} \right)_{j-\frac{1}{2}}^+ \right).
\end{aligned}$$

Adding the latter two equalities and summing over j , we get

$$-\frac{\sqrt{2}}{v_{th}^2} \left[\frac{1}{2 v_{th}} \frac{d}{dt} \int_0^L E^2 \, dx - \int_0^L \frac{\partial C_0}{\partial t} \Phi \, dx \right] = \frac{\sqrt{2}}{v_{th}^3} \sum_j \left(\left[\Phi \frac{\partial E}{\partial t} \right] - \frac{\partial \widehat{E}}{\partial t} [\Phi] - \hat{\Phi} \left[\frac{\partial E}{\partial t} \right] \right)_{j-\frac{1}{2}}.$$

Again using that,

$$\begin{aligned}
\left[\Phi \frac{\partial E}{\partial t} \right] - \frac{\partial \widehat{E}}{\partial t} [\Phi] - \hat{\Phi} \left[\frac{\partial E}{\partial t} \right] &= \left(\{\Phi\} - \hat{\Phi} \right) \left[\frac{\partial E}{\partial t} \right] + \left(\left\{ \frac{\partial E}{\partial t} \right\} - \frac{\partial \widehat{E}}{\partial t} \right) [\Phi] \\
&= \beta \left[\frac{\partial \Phi}{\partial t} \right] [\Phi] \\
&= \frac{\beta}{2} \frac{d}{dt} [\Phi]^2,
\end{aligned}$$

we get the time derivative of the discrete potential energy,

$$(3.14) \quad \frac{1}{\sqrt{2} v_{th}^3} \frac{d}{dt} \left[\int_0^L E^2 \, dx + \beta \sum_j [\Phi]_{j-\frac{1}{2}}^2 \right] = \frac{\sqrt{2}}{v_{th}^2} \int_0^L \frac{\partial C_0}{\partial t} \Phi \, dx.$$

Gathering (3.12), (3.13) and (3.14) in (3.11), we get

$$\frac{d}{dt} \left[\int_0^L \left(C_2 + \frac{1}{\sqrt{2} v_{th}^3} E^2 \right) dx + \frac{\beta}{\sqrt{2} v_{th}^3} \sum_j [\Phi]_{j-\frac{1}{2}}^2 \right] = 0.$$

Finally, using the conservation of mass and the latter result, we get the conservation of discrete energy

$$\frac{1}{2} \frac{d}{dt} \left[\int_0^L v_{th}^3 \left(\sqrt{2} C_2 + C_0 \right) + |E|^2 dx + \beta \sum_j [\Phi]_{j-\frac{1}{2}}^2 \right] = 0.$$

□

Remark 3.2. *It is possible to apply the same method considering the symmetrically weighted basis with the $L^2(\mathbb{R})$ norm in order to design a conservative discontinuous Galerkin method. However, the residue (r_1, r_2) would involve all the modes $(C_n)_{0 \leq n < N_H}$ causing an additional computational cost. This is the main reason why we favor the asymmetrically weighted basis.*

3.3. Time discretization. In this section, we propose a time discretization to the modified semi-discrete scheme (3.1)-(3.5), with (3.6)-(3.7) to ensure the conservation of momentum and energy. As it has been shown in the proof of Proposition 3.1, the conservation of momentum can be obtained by a simple modification of the source term, whereas the conservation of energy is more tricky since it involves time derivative. Therefore, the time discretization is an issue for the conservation of energy.

We denote by $\mathbf{C} = (C_0, \dots, C_{N_H-1})$ the solution to (3.1)-(3.7) and by (\cdot, \cdot) the standard L^2 inner product on the interval $(0, L)$

$$(C_n, \phi) := \int_0^L C_n \phi dx$$

and $(\cdot, \cdot)_I$ the standard L^2 inner product on the interval I

$$(C_n, \phi)_I := \int_I C_n \phi dx.$$

Then for the computation of the source terms, we introduce b_n^j given by,

$$b_n^j(\mathbf{C}, E, \Phi, \phi_n) = \begin{cases} 0, & \text{if } n = 0, \\ -\frac{1}{v_{th}} (E C_0, \phi_1)_{I_j} - \langle r_1^j, \phi_1 \rangle, & \text{if } n = 1, \\ -\frac{\sqrt{2}}{v_{th}} (E C_1, \phi_2)_{I_j} - \langle r_2^j, \phi_2 \rangle, & \text{if } n = 2, \\ -\frac{\sqrt{n}}{v_{th}} (E C_{n-1}, \phi_n)_{I_j}, & \text{if } 3 \leq n \leq N_H - 1, \end{cases}$$

where (r_1, r_2) is defined in (3.7). We set $a_n = \sum_j a_n^j$ and $b_n = \sum_j b_n^j$. Using these notations, the semi-discrete system (3.1)-(3.7) can be written in the compact form for the time evolution of $(C_n)_{0 \leq n < N_H}$,

$$(3.15) \quad \frac{d}{dt} (C_n, \phi_n) + a_n(g_n, \phi_n) + b_n(\mathbf{C}, E, \Phi, \phi_n) = 0, \quad \forall \phi_n \in V_h^k,$$

coupled with the local discontinuous Galerkin scheme for the Poisson equation (3.4)-(3.5).

We now present a first and second order time discretizations to (3.15) preserving the conservation properties. For simplicity we fix an interval I , for which we drop the index j and choose a time step Δt . We compute an approximation $\mathbf{C}^m = (C_0^m, \dots, C_{N_H-1}^m)$ of the solution \mathbf{C} at time $t^m = m \Delta t$, for $m \geq 0$.

First order scheme. We first apply a classical explicit Euler scheme for any $n \in \{0, \dots, N_H - 1\} \setminus \{2\}$ and $m \geq 0$,

$$(3.16) \quad \frac{(C_n^{m+1} - C_n^m, \phi_n)}{\Delta t} + a_n(g_n^m, \phi_n) + b_n(\mathbf{C}^m, E^m, \Phi^m, \phi_n) = 0, \quad \forall \phi_n \in V_h^k.$$

From this system, we get the discrete density C_0^{m+1} at time t^{m+1} and can apply the local discontinuous Galerkin scheme (3.4)-(3.5) for the computation of the electric field and potential (E^{m+1}, Φ^{m+1}) , hence we compute

$$E^{m+\frac{1}{2}} = \frac{1}{2} (E^m + E^{m+1}), \quad \Phi^{m+\frac{1}{2}} = \frac{1}{2} (\Phi^m + \Phi^{m+1}),$$

and the unknown C_2^{m+1} , given by

$$(3.17) \quad \frac{(C_2^{m+1} - C_2^m, \phi_2)}{\Delta t} + a_2(g_2^m, \phi_2) + b_2(\mathbf{C}^m, E^{m+\frac{1}{2}}, \Phi^{m+\frac{1}{2}}, \phi_2) = 0, \quad \forall \phi_2 \in V_h^k.$$

Now let us prove mass, momentum and energy conservation for this fully discrete scheme, under periodic or compact support boundary conditions.

Proposition 3.3. *For any $N_H \geq 3 \in \mathbb{N}$, we consider the solution $(\mathbf{C}^m, E^m, \Phi^m)_m$ to the system (3.16)-(3.17). Then, discrete mass and momentum are conserved for any $m \geq 0$,*

$$v_{th}^{k+1} \int_0^L C_k^m dx = v_{th}^{k+1} \int_0^L C_k^0 dx, \quad k = 0, 1$$

and the discrete total energy, defined as

$$\mathcal{E}_h^m := \frac{1}{2} \int_0^L v_{th}^3 (\sqrt{2} C_2^m + C_0^m) + |E^m|^2 dx + \frac{1}{2} \beta \sum_j [\Phi^m]_{j-\frac{1}{2}}^2,$$

is also preserved with respect to $m \geq 0$.

Proof. The conservation of mass and momentum follows the lines of the proof in Proposition 3.1, since we have by construction

$$\sum_j a_0^j(g_0^m, 1) = 0, \quad \text{and} \quad \sum_j a_1^j(g_1^m, 1) = \sum_j b_1^j(\mathbf{C}^m, E^m, \Phi^m, 1) = 0.$$

For the conservation of the total energy, we also proceed as in Proposition 3.1. We first have

$$\sum_j a_2^j(g_2^m, 1) = 0,$$

and also

$$\sum_j b_2^j(\mathbf{C}^m, E^{m+\frac{1}{2}}, \Phi^{m+\frac{1}{2}}, 1) = -\frac{\sqrt{2}}{v_{th}} \left((E^{m+\frac{1}{2}}, C_1^m) + \sum_j (\{C_1^m\} - \hat{C}_1^m) [\Phi^{m+\frac{1}{2}}]_{j-\frac{1}{2}} \right).$$

Then using the scheme for the Poisson equation (3.4) with $\eta = C_1^m$ and the scheme (3.16) for C_0^{m+1} with $\phi_0 = \Phi^{m+\frac{1}{2}}/v_{th}$, we obtain

$$\frac{(C_2^{m+1} - C_2^m, 1)}{\Delta t} = -\sum_j b_2^j(\mathbf{C}^m, E^{m+\frac{1}{2}}, \Phi^{m+\frac{1}{2}}, 1) = -\frac{\sqrt{2}}{v_{th}^2} \int_0^L \frac{C_0^{m+1} - C_0^m}{\Delta t} \Phi^{m+\frac{1}{2}} dx.$$

On the other hand by linearity of the scheme (3.4) for the Poisson equation, we apply the scheme to $\frac{C_0^{m+1} - C_0^m}{\Delta t}$ and choose the test function $\zeta = \sqrt{2} \Phi^{m+\frac{1}{2}}/v_{th}^3$ in the second equation and $\eta = -\frac{\sqrt{2}}{v_{th}^3} \frac{E^{m+1} - E^m}{\Delta t}$ in the first equation, it gives the variation of the discrete potential energy

$$\frac{\sqrt{2}}{v_{th}^2} \int_0^L \frac{C_0^{m+1} - C_0^m}{\Delta t} \Phi^{m+\frac{1}{2}} dx = \frac{1}{\sqrt{2} v_{th}^3} \left[\int_0^L \frac{|E^{m+1}|^2 - |E^m|^2}{\Delta t} dx + \beta \sum_j \frac{[\Phi^{m+1}]_{j-\frac{1}{2}}^2 - [\Phi^m]_{j-\frac{1}{2}}^2}{\Delta t} \right].$$

Finally gathering the previous result, it yields

$$\begin{aligned} & \int_0^L C_2^{m+1} + \frac{1}{\sqrt{2}v_{th}^3} |E^{m+1}|^2 dx + \frac{\beta}{\sqrt{2}v_{th}^3} \sum_j [\Phi^{m+1}]_{j-\frac{1}{2}}^2 \\ &= \int_0^L C_2^m + \frac{1}{\sqrt{2}v_{th}^3} |E^m|^2 dx + \frac{\beta}{\sqrt{2}v_{th}^3} \sum_j [\Phi^m]_{j-\frac{1}{2}}^2 \end{aligned}$$

and from the conservation of mass, we get the conservation of numerical total energy

$$\begin{aligned} & \frac{1}{2} \left[\int_0^L v_{th}^3 (\sqrt{2} C_2^{m+1} + C_0^{m+1}) + |E^{m+1}|^2 dx + \beta \sum_j [\Phi^{m+1}]_{j-\frac{1}{2}}^2 \right] \\ &= \frac{1}{2} \left[\int_0^L v_{th}^3 (\sqrt{2} C_2^m + C_0^m) + |E^m|^2 dx + \beta \sum_j [\Phi^m]_{j-\frac{1}{2}}^2 \right]. \end{aligned}$$

□

Second order scheme. Let us extend the previous scheme to second order. We first apply a classical explicit Euler scheme with a half-time step $\Delta t/2$ for any $n \in \{0, \dots, N_H - 1\} \setminus \{2\}$ and $m \geq 0$,

$$(3.18) \quad \frac{2(C_n^{(1)} - C_n^m, \phi_n)}{\Delta t} + a_n(g_n^m, \phi_n) + b_n(\mathbf{C}^m, E^m, \Phi^m, \phi_n) = 0, \quad \forall \phi_n \in V_h^k.$$

From this system, we get the discrete density $C_0^{(1)}$ at time $t^{m+\frac{1}{2}} = t^m + \Delta t/2$ and can apply (3.4)-(3.5) for the computation of the electric field and potential $(E^{(1)}, \Phi^{(1)})$ with the source term $C_0^{(1)}$, hence we compute the unknown $C_2^{(1)}$, given by

$$(3.19) \quad \frac{2(C_2^{(1)} - C_2^m, \phi_2)}{\Delta t} + a_2(g_2^m, \phi_2) + b_2\left(C^m, E^{m+\frac{1}{4}}, \Phi^{m+\frac{1}{4}}, \phi_n\right) = 0, \quad \forall \phi_2 \in V_h^k,$$

with

$$E^{m+\frac{1}{4}} = \frac{1}{2} (E^m + E^{(1)}), \quad \Phi^{m+\frac{1}{4}} = \frac{1}{2} (\Phi^m + \Phi^{(1)}).$$

Then we compute a second stage with a time step Δt for any $n \in \{0, \dots, N_H - 1\} \setminus \{2\}$ and $m \geq 0$,

$$(3.20) \quad \frac{(C_n^{m+1} - C_n^m, \phi_n)}{\Delta t} + a_n(g_n^{(1)}, \phi_n) + b_n(\mathbf{C}^{(1)}, E^{(1)}, \Phi^{(1)}, \phi_n) = 0, \quad \forall \phi_n \in V_h^k.$$

From this system, we get the discrete density C_0^{m+1} at time $t^{m+1} = t^m + \Delta t$ and can apply the local discontinuous Galerkin scheme (3.4)-(3.5) for the computation of the electric field and potential (E^{m+1}, Φ^{m+1}) , hence we compute

$$E^{m+\frac{1}{2}} = \frac{1}{2} (E^m + E^{m+1}), \quad \Phi^{m+\frac{1}{2}} = \frac{1}{2} (\Phi^m + \Phi^{m+1}),$$

and the unknown C_2^{m+1} , given by

$$(3.21) \quad \frac{(C_2^{m+1} - C_2^m, \phi_2)}{\Delta t} + a_2(g_2^{(1)}, \phi_2) + b_2(\mathbf{C}^{(1)}, E^{m+\frac{1}{2}}, \Phi^{m+\frac{1}{2}}, \phi_n) = 0, \quad \forall \phi_2 \in V_h^k.$$

We have the following result for the second order scheme (3.18)-(3.21).

Proposition 3.4. *For any $N_H \geq 3 \in \mathbb{N}$, we consider the solution $(\mathbf{C}^m, E^m, \Phi^m)_m$ to the system (3.18)-(3.21). Then, discrete mass and momentum are conserved for any $m \geq 0$,*

$$v_{th}^{k+1} \int_0^L C_k^m dx = v_{th}^{k+1} \int_0^L C_k^0 dx, \quad k = 0, 1$$

and the discrete total energy, defined as

$$\mathcal{E}_h^m := \frac{1}{2} \int_0^L v_{th}^3 \left(\sqrt{2} C_2^m + C_0^m \right) + |E^m|^2 dx + \frac{1}{2} \beta \sum_j [\Phi^m]_{j-\frac{1}{2}}^2,$$

is also preserved with respect to $m \geq 0$.

Proof. As we can see, the first stage is the same as the first order scheme (3.16)-(3.17), but with a half time step at $t^m + \Delta t/2$, so the conservation of mass, momentum and energy is directly obtained. For the second stage, the proof is very similar, and this step directly ensures conservation of mass, momentum and energy. \square

4. NUMERICAL EXAMPLES

In this section, we will verify our proposed DG/Hermite Spectral method for the one-dimensional Vlasov-Poisson (VP) system. We take the phase domain along v to be $[-8, 8]$, with N_H modes for Hermite spectral bases, and N_x cells in space. We note that due to the Hermite spectral basis, there is no truncation error for the conservation of mass, momentum and energy from cut-off along the v -direction. The scaling velocity v_{th} is chosen to be 1 and the Hou-Li filter with 2/3 dealiasing rule [23, 12] will be used, if without specification.

In the following, we take P_2 piecewise polynomial in space and 2nd order scheme in time. We denote this scheme as ‘‘DGHSM’’. We compute reference solutions using a positivity-preserving semi-Lagrangian finite difference (SLFD) WENO scheme in [34], which is denoted as ‘‘SLFDM’’. The SLFDM uses discrete velocity coordinate, and the mesh size is $N_x \times N_v$.

4.1. Landau damping. We first consider the Landau damping problem for the VP system with the initial condition:

$$(4.1) \quad f(0, x, v) = (1 + \alpha \cos(kx)) \frac{1}{\sqrt{2\pi}} \exp\left(-\frac{v^2}{2}\right).$$

Under Hermite spectral basis in velocity, we have

$$(4.2) \quad C_0(t, x) = 1 + \alpha \cos(kx),$$

and $C_n(t, x) = 0, n \geq 1$. The background density $\rho_0 = 1$. The length of the domain in the x -direction is $L = \frac{2\pi}{k}$.

We first take $\alpha = 0.05$ with $k = 0.5$ and use this example to verify the orders of our scheme. We compute the solution to $T = 0.1$. The errors are computed by comparing to the solution on using $N_x = 512$ and P_3 piecewise polynomial bases, and $N_H = 600$. In Table 4.1, we show the L^2 errors and orders for P_k piecewise polynomials with $k = 1, 2, 3$ respectively. Due to the time steps are smaller than the spatial mesh size, we can observe $(k+1)$ -th order convergence for P_k polynomials respectively.

We then consider the weak Landau damping with $\alpha = 0.01$ and $k = 0.5$ in (4.1). We take $N_H = 256$ and $N_x = 64$ and compute the solution up to $T = 60$. We show the time evolution of the relative deviations of discrete mass, momentum and total energy in Figure 4.1 (left). We can see the errors for these three conservative quantities are up to machine precision, which demonstrate that the scheme can preserve exact mass, momentum and energy. We plot the time evolution of the electric field in L^2 norm (E_2) and L^∞ norm (E_{max}) in Figure 4.1 (right). The numerical damping rate for this case matches the theoretical linear damping rate -0.1533 very well.

We also consider the strong Landau damping with $\alpha = 0.5$ and $k = 0.5$ in (4.1). Here we take $N_H = 1024$ and $N_x = 64$ and compute the solution up to $T = 60$. Time evolution of the relative deviations of discrete mass, momentum and total energy are reported in Figure 4.2 (left). Similarly these errors are up to machine precision. We also plot the time evolution of the electric field in L^2 norm (E_2) and L^∞ norm (E_{max}) in Figure 4.2 (right). We compare the electric field to the one obtained by the SLFD WENO scheme with mesh size 256×512 . We can see that the results match each other. We show the surface plots of the distribution function at $T = 40$ for both methods, and they are also very similar.

TABLE 4.1. Numerical L^2 errors and orders for Landau damping with initial distribution (4.1). $\alpha = 0.05$ and $k = 0.5$. $T = 0.1$. $N_H = 600$.

N_x	P_1		P_2		P_3	
	L^2 error	Order	L^2 error	Order	L^2 error	Order
32	1.81E-4	–	4.88E-6	–	1.43E-07	–
64	4.53E-5	2.00	5.65E-7	3.11	1.24E-08	3.53
128	1.17E-5	1.95	6.22E-8	3.18	7.84E-10	3.98
256	3.17E-6	1.88	6.94E-9	3.16	4.96E-11	3.98

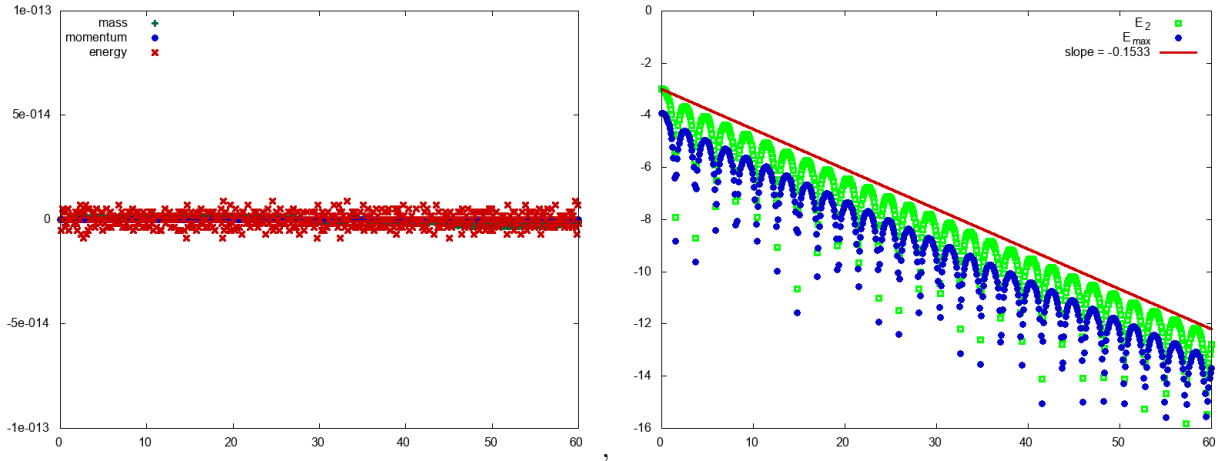


FIGURE 4.1. Weak Landau damping of the initial distribution (4.1) with $\alpha = 0.01$ and $k = 0.5$. $T = 60$. Left: deviation of mass, momentum and energy. Right: time evolution of the electric field in L^2 norm (E_2) and L^∞ norm (E_{max}) (logarithmic value). Mesh size: $N_x \times N_H = 64 \times 256$.

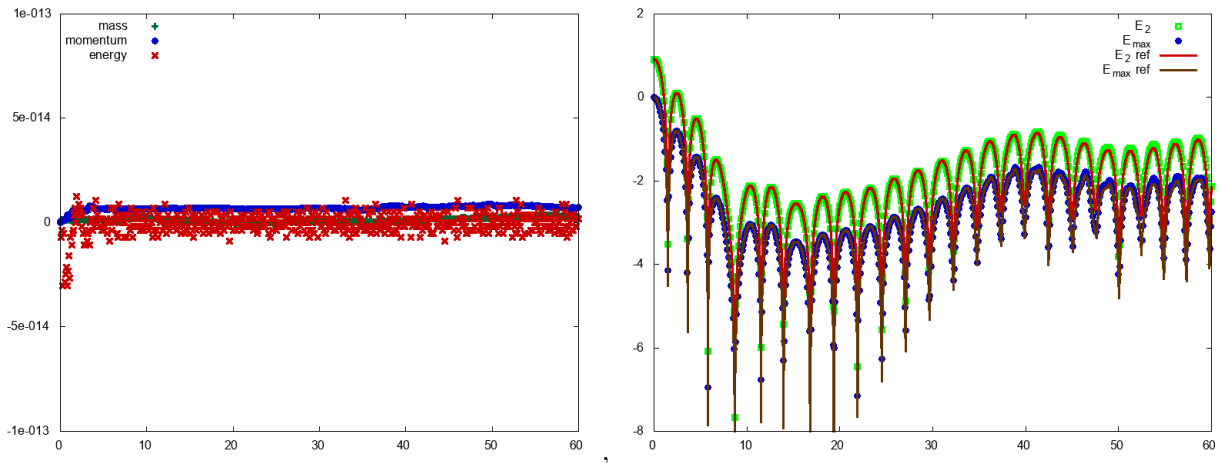


FIGURE 4.2. Strong Landau damping of the initial distribution (4.1) with $\alpha = 0.5$. $T = 60$. Left: deviation of mass, momentum and energy. Right: time evolution of the electric field in L^2 norm (E_2) and L^∞ norm (E_{max}) (logarithmic value). DGFSM: $N_x \times N_H = 64 \times 1024$. The reference solution is from SLFDM with $N_x \times N_v = 256 \times 512$.

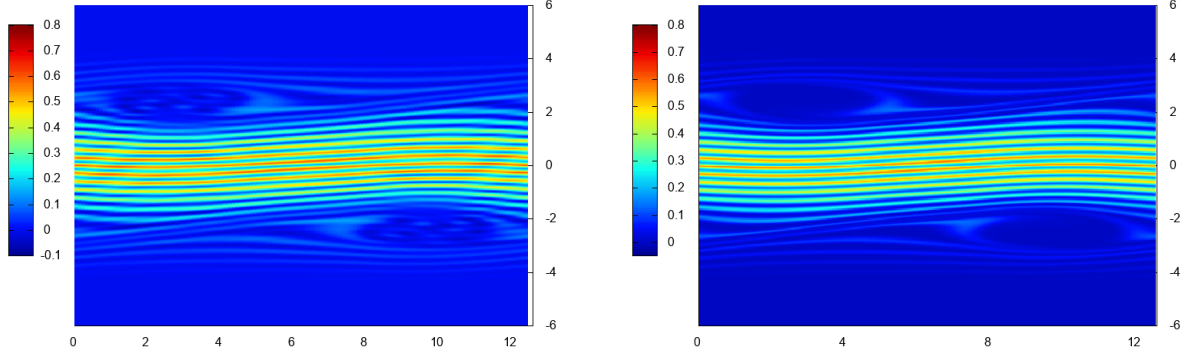


FIGURE 4.3. Strong Landau damping of the initial distribution (4.1) with $\alpha = 0.5$ and $k = 0.5$. Surface plot of the distribution function at $T = 40$. Left: $N_x \times N_H = 64 \times 1024$ for DGHSM; right: $N_x \times N_v = 256 \times 512$ for SLFDM.

4.2. Two stream instability. In this example, we consider the two stream instability problem with the initial distribution function

$$(4.3) \quad f(0, x, v) = \frac{2}{7}(1 + 5v^2)(1 + \alpha((\cos(2kx) + \cos(3kx))/1.2 + \cos(kx))) \frac{1}{\sqrt{2\pi}} \exp\left(-\frac{v^2}{2}\right),$$

where $\alpha = 0.01$ and $k = 0.5$. For this case, we have

$$\begin{cases} C_0(t, x) = \frac{12}{7}(1 + \alpha((\cos(2kx) + \cos(3kx))/1.2 + \cos(kx))), \\ C_2(t, x) = \frac{10\sqrt{2}}{7}(1 + \alpha((\cos(2kx) + \cos(3kx))/1.2 + \cos(kx))). \end{cases}$$

Other $C_n(t, x)$'s are all zero and $\rho_0 = 12/7$. Similarly $L = \frac{2\pi}{k}$.

We compute the solution up to time $T = 60$. For DGHSM, we take $N_x = 64$ and $N_H = 256$. We show the time evolution of the relative deviations of discrete mass, momentum and total energy in Figure 4.4 (left). We can see these errors are still up to machine precision. Although the momentum decreases a little, the errors are at the level of 10^{-13} . We also plot the time evolution of the electric field in L^2 norm (E_2) and L^∞ norm (E_{max}) in Figure 4.4 (right). We compare them with the results from SLFDM on the mesh 256×512 , and they match each other very well. For this case, we show the surface plots of f at $T = 50$ in Figure 4.5 for both methods. The results are comparable, only very weak high frequency instabilities are observed localized in the center for DGFSM.

4.3. Bump-on-tail instability. Lastly we consider the bump-on-tail instability problem with the initial distribution as

$$(4.4) \quad f(0, x, v) = f_{b.o.t}(v)(1 + \alpha \cos(k n x)),$$

where the bump-on-tail distribution is

$$(4.5) \quad f_{b.o.t}(v) = \frac{n_p}{\sqrt{\pi}v_{th,p}} \exp\left(-\frac{v^2}{v_{th,p}^2}\right) + \frac{n_b}{\sqrt{\pi}v_{th,b}} \exp\left(-\frac{(v - v_{d,b})^2}{v_{th,b}^2}\right).$$

We first choose the parameters to be $n_p = 0.99$, $n_b = 0.01$, $v_{d,b} = 1$, $v_{th,p} = 0.28284271$, $v_{th,b} = 7.0710678E-02$, $\alpha = 0.0001$, $n = 10$ and $k = 0.1$. The computational domain is $[0, \frac{2\pi}{k}] \times [-8, 8]$. The settings are the same as in [29] (Table 7). For this case with a small perturbation $\alpha = 0.0001$, we do not apply the Hou-Li filter to avoid numerical dissipation.

We compute the solution up to time $T = 200$ with $N_x = 64$ and $N_H = 256$. The time evolution of the relative deviations of discrete mass, momentum and total energy are reported in Figure 4.6 (left). We can see these errors are up to machine precision for this long time simulation. We also plot the

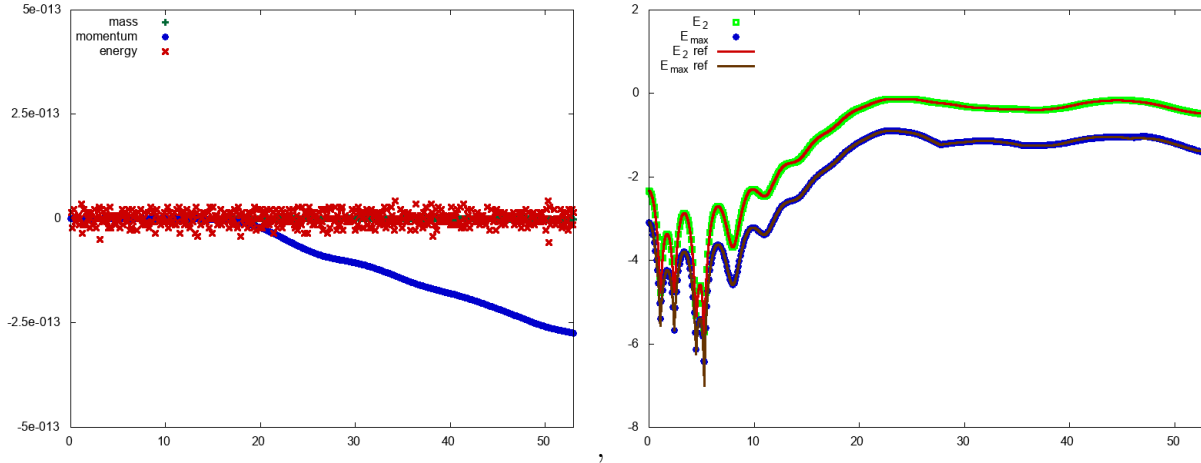


FIGURE 4.4. Two stream instability of the initial distribution (4.3) with $\alpha = 0.01$ and $k = 0.5$. Left: deviation of mass, momentum and energy. Right: time evolution of the electric field in L^2 norm (E_2) and L^∞ norm (E_{max}) (logarithmic value). DGFSM: $N_x \times N_H = 128 \times 512$. The reference solution is from SLFDM with $N_x \times N_v = 256 \times 512$.

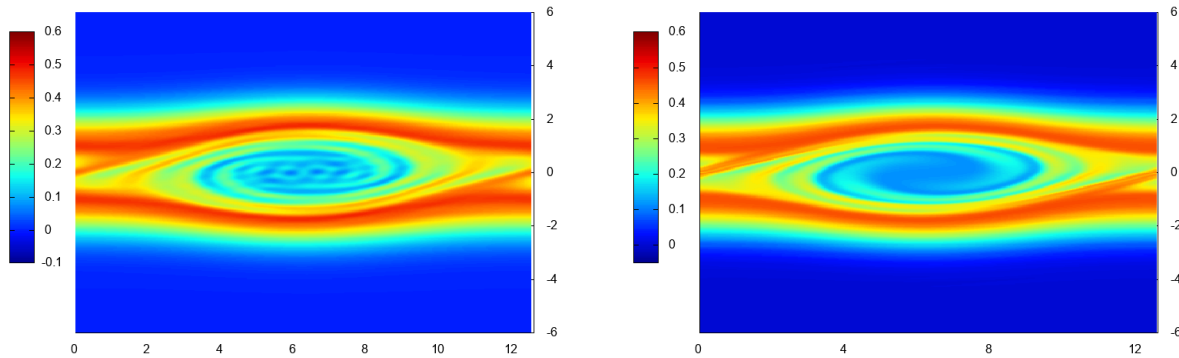


FIGURE 4.5. Two stream instability of the initial distribution (4.3) with $\alpha = 0.01$ and $k = 0.5$. Surface plot of the distribution function f at $T = 50$. Left: $N_x \times N_H = 128 \times 512$ for DGFSM; right: $N_x \times N_v = 256 \times 512$ for SLFDM.

time evolution of the electric field in L^2 norm (E_2) and L^∞ norm (E_{max}) in Figure 4.6 (right). We compare them to the results by using the SLFD WENO method with mesh size 256×512 . We can see they match each other very well. Besides both of them have a growing rate very close to 0.1084353 from the linear theory [29].

Secondly, we consider a strong perturbation with $\alpha = 0.04$, $n = 3$ and $k = 0.1$. Other parameters are set to be $n_p = 0.9$, $n_b = 0.1$, $v_{d,b} = 4.5$, $v_{th,p} = \sqrt{2}$, $v_{th,b} = \sqrt{2}/2$. The computational domain is still $[0, \frac{2\pi}{k}] \times [-8, 8]$. These settings have been used in [28, 34]. For this case, the Hou-Li filter is used and besides we take the scaling velocity $v_{th} = 1.4$.

We take $N_x \times N_H = 128 \times 512$ for DGFSM and compare the solutions to SLFDM with $N_x \times N_v = 160 \times 320$. We first show the time evolution of the relative deviations of discrete mass, momentum and total energy in Figure 4.7 (top left). These errors are also up to machine precision. We also plot the time evolution of the electric field in L^2 norm (E_2) and L^∞ norm (E_{max}) in Figure 4.7 (top right), as well as the time evolution of the total electric energy in Figure 4.7 (bottom). We compare them to the results by using the SLFD WENO method with mesh size 160×320 . We can see these results have the same structure and they are similar to those in [28]. Finally we show the surface plots of the

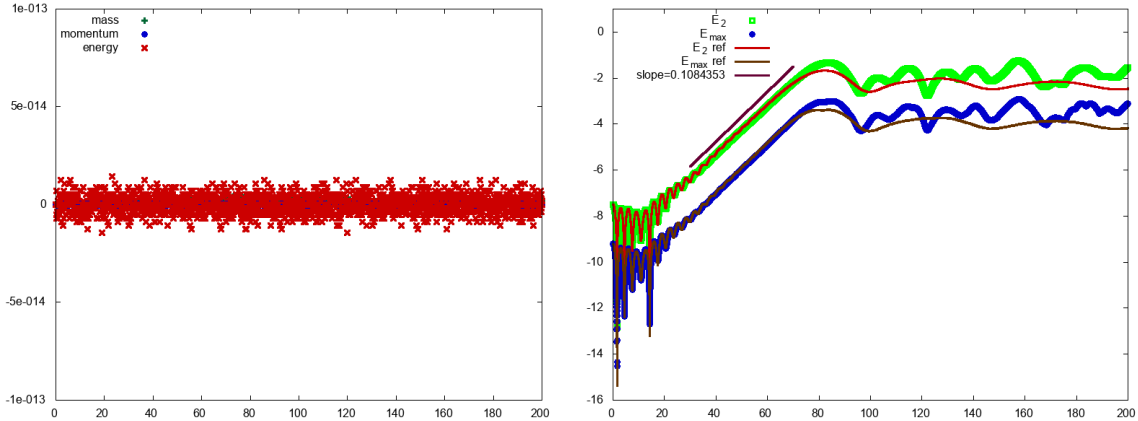


FIGURE 4.6. Bump-on-tail instability with the initial condition (4.4) for a small perturbation $\alpha = 0.0001$. $k = 0.1$ and $n = 10$. Left: deviation of mass, momentum and energy. Right: time evolution of the electric field in L^2 norm (E_2) and L^∞ norm (E_{max}) (logarithmic value). DGFSM: $N_x \times N_H = 64 \times 256$. The reference solution is from SLFDM with $N_x \times N_v = 160 \times 1024$.

distribution function at $T = 20, 50, 200$ in Figure 4.8. From the comparison of these two methods, we can find that at the beginning $T = 20$, the solutions are very close. But as time evolves, the solutions are moving in different phases. However, the results from DGFSM look relatively well.

5. CONCLUSION AND PERSPECTIVES

In this paper, we introduced a new method to solve the Vlasov equation using Hermite polynomials for the velocity variable and discontinuous Galerkin methods for space discretization. This method enforces the conservation of global mass, momentum and energy. A filtering algorithm allows to control spurious oscillations without affecting the conservation properties. Therefore, our approach allows to treat strong nonlinear problems without generating numerical instabilities. Numerical results show that our scheme is as accurate as semi-lagrangian methods and the local reconstruction is well suited to do parallel computation in high dimension.

The main advantage of the present approach, using Hermite functions for the velocity variable, is that it provides the evolution of macroscopic quantities, that is, density, momentum, energy and higher order moment in velocity of the distribution function. Of course, it would be interesting to adapt the number of moments during the time evolution according to the variations of the distribution function as in [27]. In a further study we would like to investigate the extension to the Vlasov-Maxwell system and the coupling of this algorithm with fluid solvers in order to solve the kinetic equation only where it is useful [15, 18].

ACKNOWLEDGEMENT

Francis Filbet is supported by the EUROfusion Consortium and has received funding from the Euratom research and training programme 2014-2018 under grant agreement No 633053. The views and opinions expressed herein do not necessarily reflect those of the European Commission.

T. Xiong acknowledges support by NSFC grant No. 11971025, NSF grant of Fujian Province No. 2019J06002 and NSAF No. U1630247.

This work started when the first author visited the Tianyuan Mathematical Center in Southeast China at Xiamen University in June 2019 for a research group discussion. The author would like to thank the Tianyuan Mathematical Center for its hospitality.

CONFLICT OF INTEREST

On behalf of all authors, the corresponding author states that there is no conflict of interest.

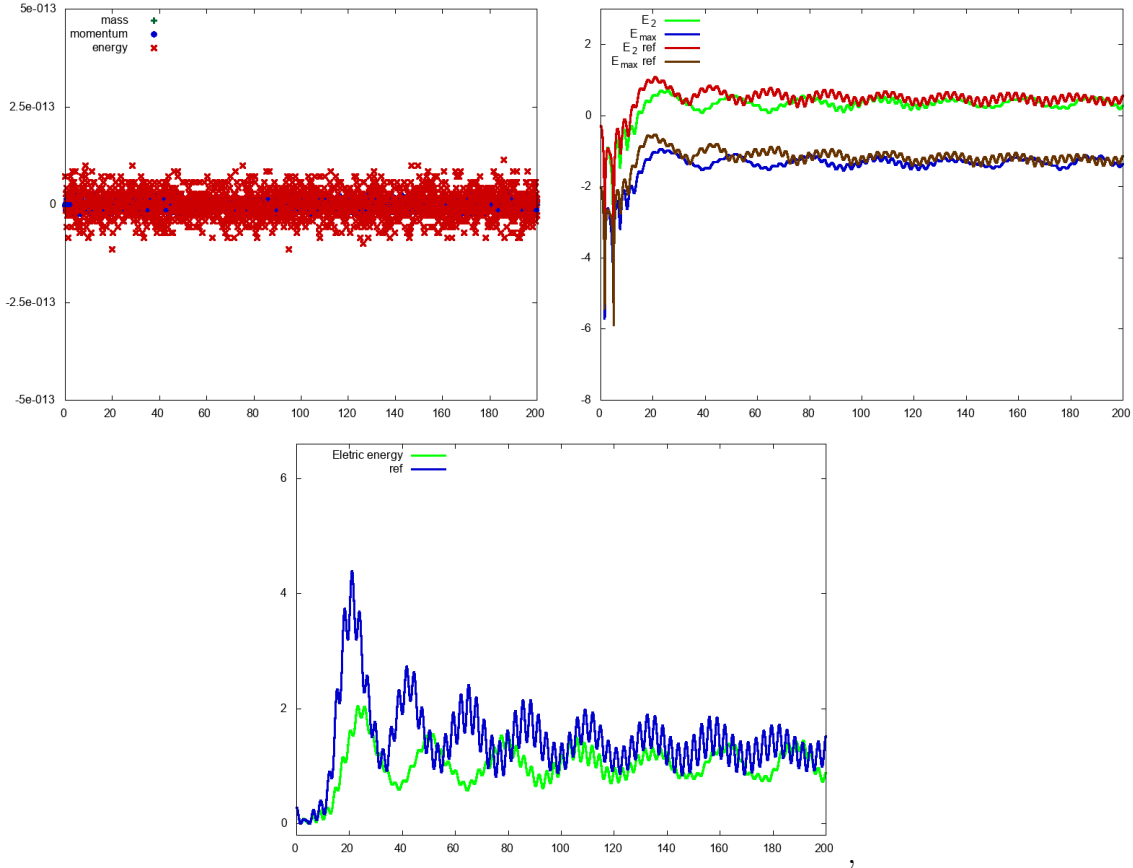


FIGURE 4.7. Bump-on-tail instability with the initial condition (4.4) for a strong perturbation $\alpha = 0.04$. $k = 0.1$ and $n = 3$. Top left: deviation of mass, momentum and energy. Top right: time evolution of the electric field in L^2 norm (E_2) and L^∞ norm (E_{max}) (logarithmic value). Bottom: time evolution of the electric energy. DGFSM: $N_x \times N_H = 128 \times 512$. The reference solution is from SLFDM with $N_x \times N_v = 160 \times 320$.

REFERENCES

- [1] T. P. Armstrong. Numerical studies of the nonlinear Vlasov equation. *The Physics of Fluids*, 10(6):1269–1280, 1967.
- [2] B. Ayuso, J. A. Carrillo, and C.-W. Shu. Discontinuous Galerkin methods for the one-dimensional Vlasov-Poisson system. *Kinetic and Related Models*, 4:955–989, 2011.
- [3] B. Ayuso, J. A. Carrillo, and C.-W. Shu. Discontinuous Galerkin methods for the multi-dimensional Vlasov-Poisson problem. *Mathematical Models and Methods in Applied Sciences*, 22(12):1250042, 2012.
- [4] C. K. Birdsall and A. B. Langdon. Plasma Physics via Computer Simulation. *Institute of Physics, CRC Press*, 2004.
- [5] D. L. Book and J. P. Boris. Computational Techniques for Solution of Convective Equations. In *Finite-Difference Techniques for Vectorized Fluid Dynamics Calculations*, Springer Series in Computational Physics, pages 5–28. Springer, New York, 1981.
- [6] J. P. Boyd. *Chebyshev and Fourier Spectral Methods*. Courier Corporation, 2001.
- [7] Z. Cai, R. Li, and Y. Wang. Solving Vlasov equations using NRxx method. *SIAM Journal on Scientific Computing*, 35(6):A2807–A2831, 2013.
- [8] Z. Cai and Y. Wang. Suppression of recurrence in the Hermite-spectral method for transport equations. *SIAM Journal on Numerical Analysis*, 56(5):3144–3168, 2018.
- [9] E. Camporeale, G. L. Delzanno, B. Bergen, and J. D. Moulton. On the velocity space discretization for the Vlasov-Poisson system: Comparison between implicit Hermite spectral and Particle-in-Cell methods. *Computer Physics Communications*, 198:47–58, 2016.
- [10] Y. Cheng, I. M. Gamba, F. Li, and P. J. Morrison. Discontinuous Galerkin methods for the Vlasov-Maxwell equations. *SIAM Journal on Numerical Analysis*, 52(2):1017–1049, 2014.
- [11] Y. Cheng, I. M. Gamba, and P. J. Morrison. Study of conservation and recurrence of Runge-Kutta discontinuous Galerkin schemes for Vlasov-Poisson systems. *Journal of Scientific Computing*, 56(2):319–349, 2013.

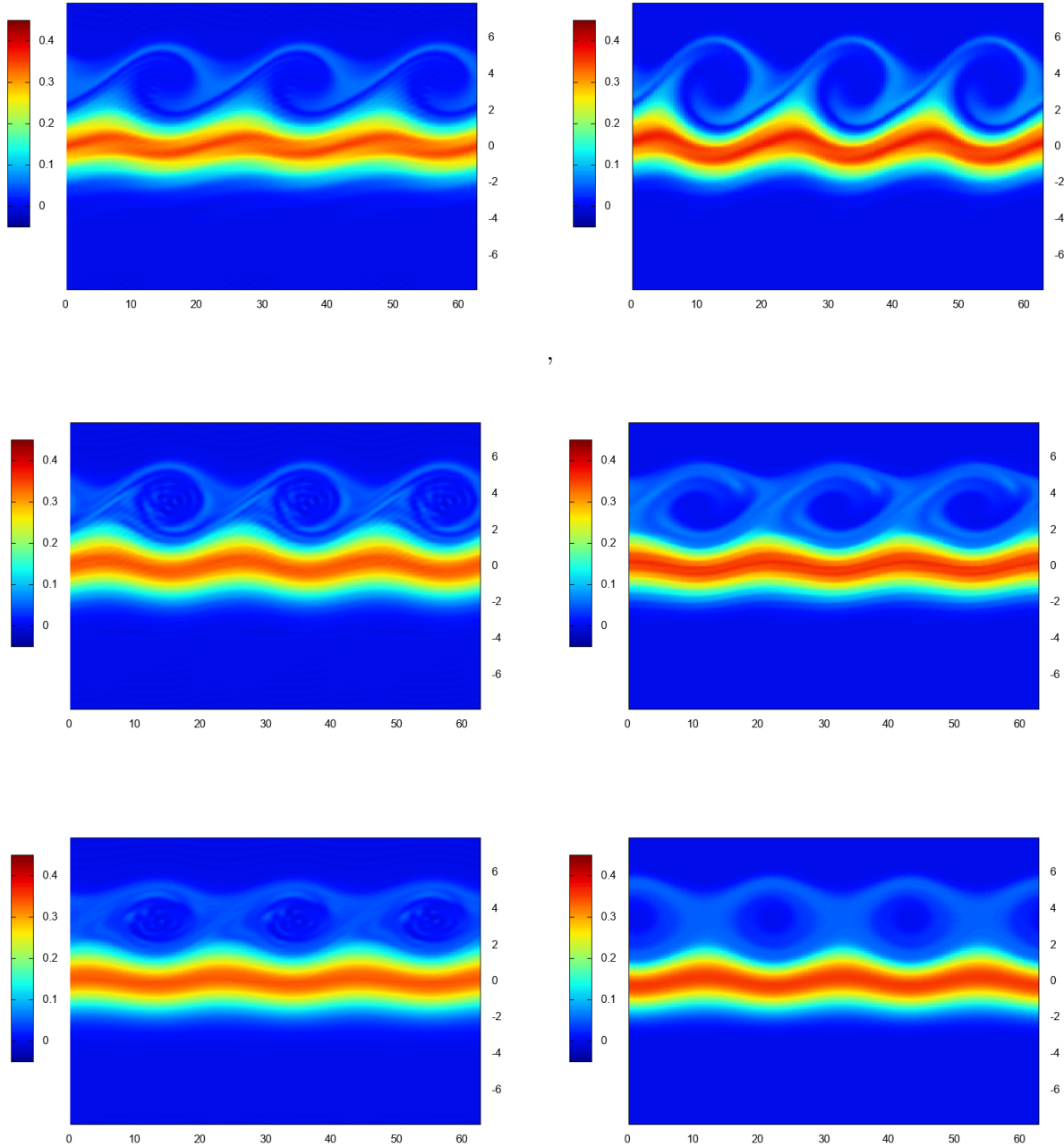


FIGURE 4.8. Bump-on-tail instability with the initial condition (4.4) for a strong perturbation $\alpha = 0.04$. $k = 0.1$ and $n = 3$. Surface plots of the distribution function f at $T = 20, 50, 200$ (from top to bottom). Left: $N_x \times N_H = 128 \times 512$ for DGFSM; right: $N_x \times N_v = 160 \times 320$ for SLFDM.

- [12] Y. Di, Y. Fan, Z. Kou, R. Li, and Y. Wang. Filtered Hyperbolic Moment Method for the Vlasov Equation. *Journal of Scientific Computing*, 79(2):969–991, 2019.
- [13] R. Ducloux, B. Dubroca, F. Filbet, and V. Tikhonchuk. High order resolution of the Maxwell-Fokker-Planck-Landau model intended for ICF applications. *Journal of Computational Physics*, 228(14):5072–5100, 2009.
- [14] B. Eliasson. Numerical modelling of the two-dimensional Fourier transformed Vlasov–Maxwell system. *Journal of Computational Physics*, 190(2):501–522, 2003.

- [15] F. Filbet and T. Rey. A hierarchy of hybrid numerical methods for multiscale kinetic equations. *SIAM Journal on Scientific Computing*, 37(3):A1218–A1247, 2015.
- [16] F. Filbet and E. Sonnendrücker. Comparison of Eulerian Vlasov solvers. *Computer Physics Communications*, 150(3):247–266, 2003.
- [17] F. Filbet, E. Sonnendrücker, and P. Bertrand. Conservative numerical schemes for the Vlasov equation. *Journal of Computational Physics*, 172(1):166–187, 2001.
- [18] F. Filbet and T. Xiong. A hybrid discontinuous Galerkin scheme for multi-scale kinetic equations. *Journal of Computational Physics*, 372:841–863, 2018.
- [19] D. Funaro and O. Kavian. Approximation of some diffusion evolution equations in unbounded domains by Hermite functions. *Mathematics of Computation*, 57(196):597–619, 1991.
- [20] R. E. Heath, I. M. Gamba, P. J. Morrison, and C. Michler. A discontinuous Galerkin method for the Vlasov-Poisson system. *Journal of Computational Physics*, 231(4):1140–1174, 2012.
- [21] J. S. Hesthaven, S. Gottlieb, and D. Gottlieb. *Spectral Methods for Time-Dependent Problems*, volume 21. Cambridge University Press, 2007.
- [22] J. P. Holloway. Spectral velocity discretizations for the Vlasov-Maxwell equations. *Transport Theory and Statistical Physics*, 25(1):1–32, 1996.
- [23] T. Y. Hou and R. Li. Computing nearly singular solutions using pseudo-spectral methods. *Journal of Computational Physics*, 226:379–397, 2007.
- [24] G. Joyce, G. Knorr, and H. K. Meier. Numerical integration methods of the Vlasov equation. *Journal of Computational Physics*, 8(1):53–63, 1971.
- [25] A. J. Klimas and W. M. Farrell. A splitting algorithm for Vlasov simulation with filamentation filtration. *Journal of Computational Physics*, 110(1):150–163, 1994.
- [26] S. Le Bourdieu, F. De Vuyst, and L. Jacquet. Numerical solution of the Vlasov–Poisson system using generalized Hermite functions. *Computer Physics Communications*, 175(8):528–544, 2006.
- [27] G. Manzini, G. L. Delzanno, J. Vencels, and S. Markidis. A Legendre–Fourier spectral method with exact conservation laws for the Vlasov–Poisson system. *Journal of Computational Physics*, 317:82–107, 2016.
- [28] M. Shoucri and G. Knorr. Numerical integration of the Vlasov equation. *Journal of Computational Physics*, 14(1):84–92, 1974.
- [29] J. W. Shumer and J. P. Holloway. Vlasov simulations using velocity-scaled Hermite representations. *Journal of Computational Physics*, 144(2):626–661, 1998.
- [30] E. Sonnendrücker, F. Filbet, A. Friedman, E. Oudet, and J.-L. Vay. Vlasov simulations of beams with a moving grid. *Computer Physics Communications*, 164(1-3):390–395, 2004.
- [31] E. Sonnendrücker, J. Roche, P. Bertrand, and A. Ghizzo. The semi-Lagrangian method for the numerical resolution of the Vlasov equation. *Journal of Computational Physics*, 149(2):201–220, 1999.
- [32] K. Takizawa, T. Yabe, and T. Nakamura. Multi-dimensional semi-Lagrangian scheme that guarantees exact conservation. *Computer Physics Communications*, 148(2):137–159, 2002.
- [33] T. Tang. The Hermite spectral method for Gaussian-type functions. *SIAM Journal on Scientific Computing*, 14(3):594–606, 1993.
- [34] T. Xiong, J.-M. Qiu, Z. Xu, and A. Christlieb. High order maximum principle preserving semi-Lagrangian finite difference WENO schemes for the Vlasov equation. *Journal of Computational Physics*, 273:618–639, 2014.
- [35] H. Yang and F. Li. Error estimates of Runge-Kutta discontinuous Galerkin methods for the Vlasov-Maxwell system. *ESAIM Mathematical Modelling and Numerical Analysis*, 49(1):69–99, 2015.

E-mail address: francis.filbet@math.univ-toulouse.fr

E-mail address: txiong@xmu.edu.cn